Proceedings of Computational Engineering Conference Vol. 28, 2023 May **JSCES**

Droplet/Aerosol Dispersion Simulation for Assessing the Infection Risk Due to Airborne Virus in a Sport Stadium Type Environment

Kim Sangwon¹⁾, Onishi Junya¹⁾, Bale Rahul¹⁾ and Tsubokura Makoto^{1,2)}

1) Ph.D, RIKEN, Center for Computational Science (7-1-26, Chuo Ward, Kobe, 650-0047, Japan)

2) Ph.D. Department of Computational Science, Kobe University (1-1 Rokkodaicho, Nada Ward, Kobe, 657-8501, Japan)

This study investigates the droplet dispersion and infection risk for airborne diseases in various seating arrangements and wind flow conditions in flat and inclined environments. A numerical framework 'CUBE', which is combined a fully compressible Navier-Stokes solver and a Lagrangian droplet dynamics model to enable large-scale parallel simulations, are utilized. This framework is built on a BCM meshing methodology to model the Eulerian mesh and decomposed Lagrangian marker particle data on each cube unit to ensure efficient parallel performance. Numerical results show that droplet dispersion and infection risk are strongly dependent on seating arrangements and wind direction. For instance, wind flow from 90° can significantly reduce local concentration of droplet dispersion and global infection risk than those of wind flow from 0°. Thus, proper seating arrangements can effectively reduce infection risk in different environments and wind flow conditions to minimize the spread of airborne diseases.

Key Words: Building-Cube Method, Dose-response model, COVID-19, Immersed boundary method, Droplet/Aerosol transmission

1. Introduction

While some airborne diseases, such as the common cold and seasonal influenza, are not very severe, several highly infectious and communicable diseases have emerged in recent decades [1, 2, 3]. In particular, as we all know, COVID-19 rapidly transformed from a local epidemic to a global pandemic since its emergence, and the usage of masks can help contain the spread of COVID-19.

However, in social situations where wearing a mask is not possible, there remains infection risk when people gather in densely packed outdoor stadiums or concert halls. In such circumstances, airborne dispersion of virus-laden sputum droplets can result in airborne disease transmission, posing a significant risk to public health. To investigate these severe situations, the numerical simulation has significant potential to predict the spread of infectious diseases in advance for various situations.

In this work, we investigate the dispersion of sputum droplets due to speaking to better understand on the dynamics of disease transmission by analyzing the effect of wind directions and velocity on infection risk. To that end, we adopt a fully compressible Navier-Stokes solver wherein the evaporated phase of the droplet and its effect on droplet evaporation is modelled [6, 7], and a discrete Lagrangian droplet model was used to model droplet transport and evaporation.

2. Governing Equations

The discretized equations for conserving mass, momentum, and energy with gas phase species reside on the Eulerian mesh. The conservation equations are provided in compact vector notation as follows:

$$\frac{\partial \mathbf{U}}{\partial t} + \nabla \cdot \mathbf{F} = \mathbf{S} \tag{1}$$

Here, the vector U and S represent the primitive flow variables and the source term, respectively, while F encompasses both the convective and diffusive terms, U and F are given below.

$$\mathbf{U} = \begin{pmatrix} \rho \\ \rho u_1 \\ \rho u_2 \\ \rho u_3 \\ \rho e \\ \rho Y_k \end{pmatrix}, \quad \mathbf{F}_i = \begin{pmatrix} \rho u_i u_1 + P \delta_{i1} - \mu A_{i1} \\ \rho u_i u_2 + P \delta_{i2} - \mu A_{i2} \\ \rho u_i u_3 + P \delta_{i3} - \mu A_{i3} \\ \rho (\rho e + P) u_i - \mu A_{ij} u_j + q_i \\ \rho u_i Y_k - \rho \hat{u}_i^k Y_k \end{pmatrix}$$
(2)

The source term S in the governing equation arises from the buoyancy term and the evaporation of droplets. The source term vector is expressed as follows:

$$\mathbf{S} = \begin{pmatrix} 0 \\ (\rho - \rho_0) \mathbf{g}_1 \\ (\rho - \rho_0) \mathbf{g}_1 \\ (\rho - \rho_0) \mathbf{g}_1 \\ (\rho - \rho_0) \mathbf{g}_i u_i \\ S_{\rho Y_k} \end{pmatrix}$$
(3)

where ρ and ρ_0 represent the local and far-field ambient densities, respectively, while **g** represents the acceleration due to gravity. $S_{\rho Y_{k}}$ represents the species source terms.

3. Droplet Equations

The single droplet model is utilized for simulating the sputum droplet dynamics. In this method, the evaporation and transport of each droplet are individually tracked. The model primarily focuses on the interaction of each droplet with the surrounding gas phase, as well as solid surfaces [8]. The governing equations for droplet transport, dispersion, and settling of the droplets are provided as below.

$$\frac{d\mathbf{x}_d}{dt} = \mathbf{u}_d \tag{4}$$

$$\frac{d\mathbf{u}_d}{dt} = \frac{3C_d}{4d_d} \frac{\rho}{\rho_d} (\mathbf{u} - \mathbf{u}_d) |\mathbf{u} - \mathbf{u}_d| + \mathbf{g}$$
 (5)

where \mathbf{u}_d , \mathbf{x}_d represent the droplet velocity and position, and the droplet drag coefficient \mathcal{C}_d is defined as a function of the droplet Reynolds number with the droplet diameter, d_d .

The droplet evaporation is modeled using the energy balance equation to monitor the droplet surface temperature and the evaporation mass flux equation. The energy balance equation is given as follows:

$$\frac{dT_d}{dt} = \frac{Nu}{3Pr} \frac{c_p}{c_l} \frac{f_1}{\tau_d} (T - T_d) + \frac{1}{m_d} \left(\frac{dm_d}{dt}\right) \frac{L_V}{c_{p,d}}$$
(6)

Here, m_d represents the mass of the droplet. T_d , and T temperature of the droplet and the ambient air, respectively. L_V denotes the latent heat of evaporation at the droplet temperature. f_1 is a correction factor for heat transfer due to droplet evaporation [9, 10]. Second, in order to evaluate the evaporation mass flux for tracking the mass of the droplet, we employ the non-equilibrium Langmuir-Knudsen model [11], and the equation is given as follows:

$$\frac{dm_d}{dt} = -\frac{m_d}{\tau_d} \left(\frac{Sh}{3Sc}\right) ln(1+B_m) \tag{7}$$

Where Sh, Sc and B_m represent the Sherwood, Schmidt numbers, and the mass transfer number, respectively. Additional information can be discovered in the studies conducted by Bale et al [6, 12].

4. Numerical Method

In this work, we employ the Building Cube Method (BCM) [13] for meshing methodology to model the Eulerian mesh as shown in Fig. 1. BCM decomposes the computational domain into discrete blocks known as cubes, which have equal sides at the same level. Based on problem requirements, larger cubes are successively subdivided into finer cubes, creating a hierarchy of smaller cubes over layers of larger cubes with a refinement ratio

of two. As a result, the cubic unit of the computational domain serves as the fundamental unit for domain decomposition during parallel computing, offering excellent scalability.

To model solid geometries immersed in the fluid, we adopt a discrete forcing immersed boundary method [14, 15]. This approach is also employed to model the sputum droplets. Here, a collection of the same sized droplet is grouped into a computational parcel. Lagrangian data structures for both cases are treated as the same discretization strategy as BCM for computational performance optimization. For domain decomposition in parallel computing, the computational domain is divided so that the Eulerian mesh and the Lagrangian marker particles spatially overlap.

We use a split time integration approach, separating the temporal integration of fluid flow equations and the species transport equations, to investigate the impact of droplet dispersion on disease spread over extensive spatial distances and long time periods. This approach is feasible if there is no strong coupling between the fluid flow and species transport equations. Therefore, the coupling mechanism for the sputum droplet modelling adopts a weak one-way coupling between the two equations. In this approach, the species transport is influenced by the fluid flow, but the species concentration remains unaffected. Moreover, to maintain numerical stability, the effect of droplet evaporation is incorporated only into the species transport equations, while the droplet source term for the fluid flow equations is ignored. This weak one-way coupling approach is frequently employed in modeling sputum droplet dispersion since the contribution of droplets to fluid flow, in terms of momentum and energy, are anticipated to be negligible[16, 17].

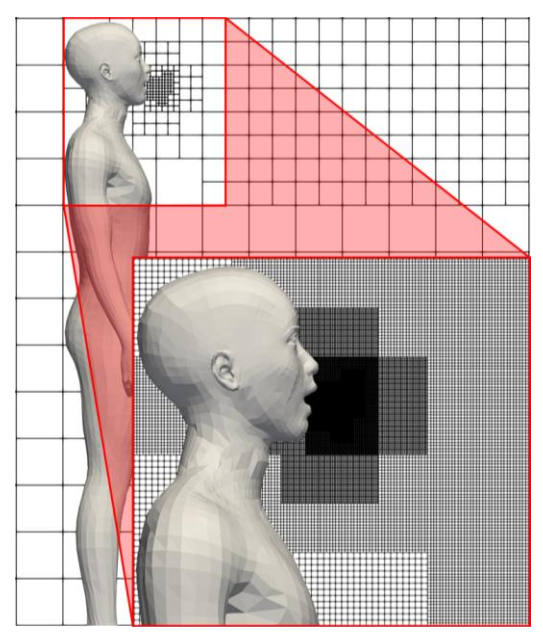


Fig. 1 Example on discretization of a computational domain into cubic blocks and subdivision of cubes into cells (close-up).

5. Sputum Droplet Modeling

This section outlines the modeling parameters for simulating sputum droplets as follows. The distribution of droplet diameters and numbers for loud speaking, adopted for the numerical simulations in this work, further details available in Bale et al. [18]. For the flow generated from the mouth during speech, we adopt a sinusoidal model, and the flow velocity over one cycle of counting from one to ten, including the two inhalations. Details can be found in the work of Gupta et al. [19]. The final parameter for the mouth opening, an average mouth opening size of 4 cm² was reported by Gupta et al. [2]. We choose a circular surface with an area of 6 cm² to model the mouth opening during speech by assuming it is larger than the opening during cough.

6. Boundary and Initial Conditions

In all cases presented in this work, the ambient air conditions are approximated as follows: 60% relative humidity, 300 K temperature and 1 atm pressure. Stagnant ambient air is applied as the initial condition for the simulations. The initial conditions for the droplets are set as follows: 0 m/s velocity, 1000 kg/m^3 density, and 307 K temperature. The droplets are driven by the flow at the time of injection to the domain. A relatively large computational domain is -25m to 25m along the x, y, and z directions. The droplet dispersion was investigated under the conditions of no wind and wind flow condition (u = 0.3 m/s).

The surface temperature of the human body is set to 300K to account for the effects of buoyancy-driven flow. For speaking simulations, the speech flow boundary condition is imposed through the mouth model. We consider the dispersion of droplets in a flat and inclined environment as shown in Fig. 2. The seating arrangements are three representative types as follows: full, staggered, and grid types. In case of the arrangement of grid type, it can be different depending on the position of the infected person. Thus, we adopted three different positions for grid type as shown in Fig. 3.

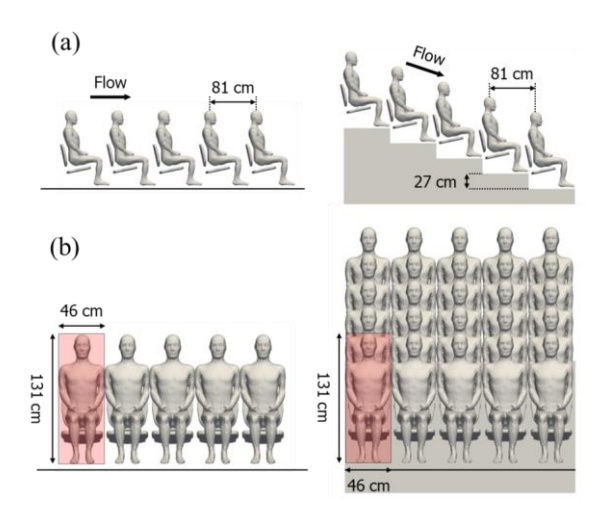


Fig. 2 Geometry as flat and inclined environments.

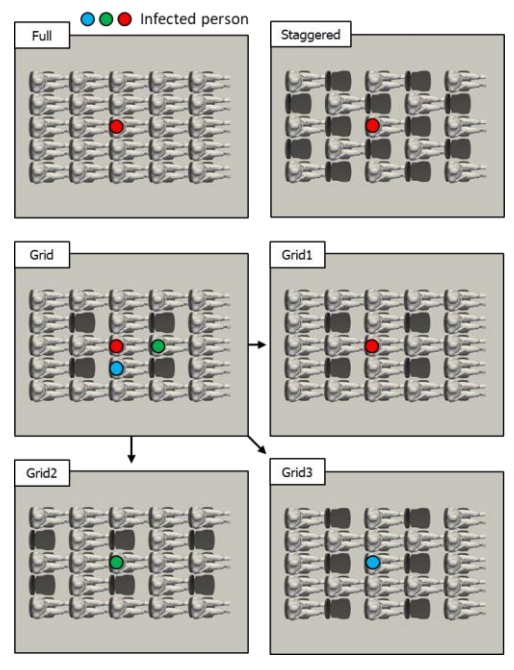


Fig. 3 Seating arrangements for full, staggered, and grid types. The grid type has three different arrangements.

7. Infection Risk Evaluation

To assess the infection probability, we used the doseresponse model [20, 21] which is widely used for quantifying the risk of airborne diseases such as COVID-19. The model assumes that the average number of viral particles needed to infect an individual is N_0 , and the infection follows a Poisson process. Thus, the probability of infection P can be expressed as

$$P = 1 - e^{\left(-\frac{N}{N_0}\right)} \tag{8}$$

where N is the total number of virions inhaled. In order to compute P, both N and N_0 must be estimated. A range of values for N_0 have been reported in some literature [22, 23]. In this study, we choose a value of 900, which lies within the reported range. The number of inhaled virions N depending on the total duration of exposure T and the amount of air inhaled by a person breathing at the rate of B, is obtain the following expression.

$$N(x,T) = \frac{B\rho_v}{v_B} \int_0^T v_d^0(t)dt$$
 (9)

In activities such as speaking and singing over extended periods, the rate of droplet generation and dispersion is expected to reach a quasi-steady state. In this state, the integral term in the above equation can be simplified to

$$N(x,T) = \frac{B\rho_v}{v_B} \bar{v}_d^0(x)T \tag{10}$$

where \bar{v}_d^0 is the quasi-steady state rate of droplet ejection volume entering the breathing zone. Further details of the model can be found in previous work [18]. Consequently, to assess the infection risk of an individual upon exposure to the droplets, the total number of droplets within the vicinity of an individual is

measured. For simplicity, a small rectangular region surrounding the mouth and nose has been chosen to represent the breathing zone. In this study, we select a $10\times10\times15\mathrm{cm}^3$ rectangular region that approximates the exhalation and inhalation volume of the speaking model. The method for tracking the droplets in the respective breathing zones are shown in Fig. 4. For simplicity, we tracked the same droplet even if it existed in the same breathing zone at the next time step or passed the previous breathing zone and entered different breathing zones.

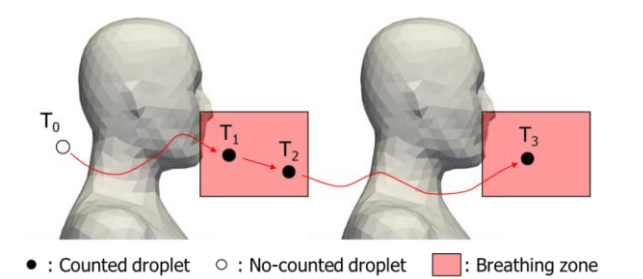


Fig. 4 A schematic of droplet tracking in the respective breathing zone.

8. Numerical Results on Infection Risk

Some snapshot of the droplet dispersion in full conditions at the flat/inclined seating arrangement is presented in Fig. 5 for no wind cases and Fig. 6 for wind blows from backside, and the droplets colored in dark blue generated by subjects. For no wind conditions, It can be seen that the dispersion of droplets can be differ as the seating environment, for instance, the droplet of a flat environment dispersed shorter distance than that of inclined conditions because the jet flow from the mouse in a flat environment is blocked by the individual front of the subject. Meanwhile, in an inclined environment, there is an open region at the front side of the subject so that the droplet disperses to the far field. In case of wind conditions, the dispersion of droplets can be different by different flow characteristics as environment induced from wind flow.

For instance, the droplet of a flat environment is dispersed in not only the front side but also the back side. This is due to the cavity and downflow generated by wind flow between the subject and the person downstream. Thus, a droplet accumulated there and propagated on the sides of the subject, and if there was a gap between the persons, the droplet spread to the backside. Meanwhile, that inclined environment only dispersed front and downside with spreading both sides than flat environments because of the open region at the front side of the subject and wind flow. The difference in the overall infection risk of individuals as two environments and wind conditions can be appreciated by comparing the infection matrices presented in Fig. 7. In this matrix, each element is corresponding with the location of each individual, the infection risk is calculated for

an exposure of 60 minutes based on the average exposure rate of a given subject to droplets and aerosols from the simulation.

As the infection matrix notes that, a clustering of infection risk around the infected subject are clearly shown. In infection risk distribution of no wind condition, both environmental conditions are shown higher risk in front of the subject. As shown by the droplet dispersion in Fig. 5, the infection risk increases from the fourth column line while increasing in front of the subject and crossing over the fifth column line in case of inclined environment. Meanwhile, in case of wind flow condition, it reduces the local concentration of droplets at the fourth column line but increases the infection risk on second and third column lines where the side and backside of the subject. Eventually, these spreading infection risks around the subject by wind flow conditions increase the global infection risk. These features that increase risk are shown in the inclined environment.

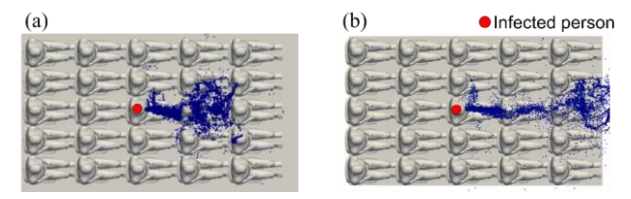


Fig. 5 Droplet dispersion in full conditions at (a) flat and (b) inclined seating arrangement, no-wind conditions.

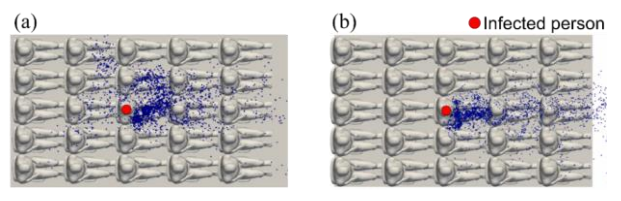


Fig. 6 Droplet dispersion in full conditions at (a) flat and (b) inclined environments, wind conditions from 0° .

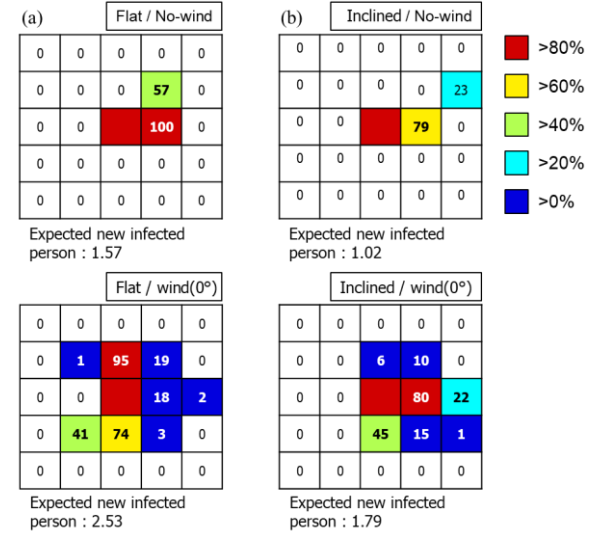


Fig. 7 Distributions of infection risk in full conditions at (a) flat and (b) inclined environment, no-wind (Top), and wind (Bottom) conditions.

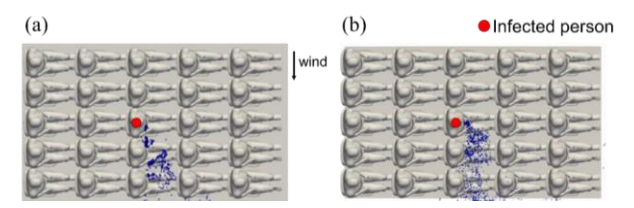


Fig. 8 Droplet dispersion in full conditions at (a) flat and (b) inclined environments, wind conditions from 0°.

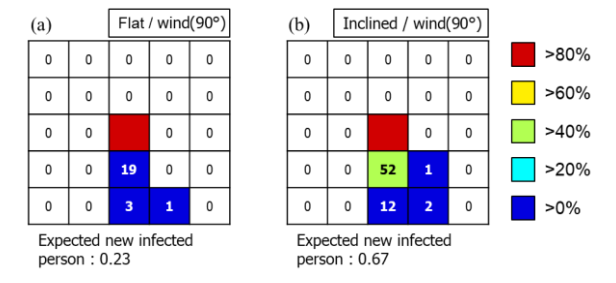


Fig. 9 Distributions of infection risk in full conditions at (a) flat and (b) inclined environment, wind conditions from 90°.

The droplet dispersion in Fig. 8 is presented on full conditions at the flat/inclined seating arrangement for wind blows from the side. The droplets in both environments are quickly transferred to the side of the subject so that is not accumulated between individuals. With this trend, global infection risk, as shown in Fig. 9, from both environments significantly decreased than those of no-wind and wind flow from the backside.

Thus, we can understand that the dispersion of droplets is strongly dependent on the wind direction. From the side view of Fig. 8, we can see that the droplet dispersed widely after passing the human models. This means that the infection risk increases somewhat as the numerical model extended. Some snapshot of the droplet dispersion in staggered conditions at the flat/inclined seating arrangement is presented in Fig. 10 for no wind cases and Fig. 11 for wind blows from backside. The infection risk for both conditions are described in Fig. 12.

For no wind conditions, both environments show a similar feature that the droplets are floated far field than those of full conditions due to the open region in front of the subject. Meanwhile, the dispersion of droplets is different as the seating environment, for example, the droplets on a flat environment and no-wind condition are accumulated in front of the individual on the fifth column line causing significant increase in infection risk. On the other hand, the trend of droplet dispersion on inclined environments and no-wind conditions is similar with those of flat and no-wind conditions, however, the difference of altitude decreases the infection risk.

In case of wind conditions, the droplet in both environments disperses on front and downside, and the cavity flows in the open region in front of the subject and the staggered seating arrangement gives space which droplet can pass through there. Eventually, the local concentration of droplets and infection risk were reduced. Meanwhile, the droplets of inclined environments are dispersed downside induced by wind so that the infection risk increases than that of no-wind conditions. Thus, proper seating arrangement can act effectively to prevent infection risk as a given environment and wind flow conditions.

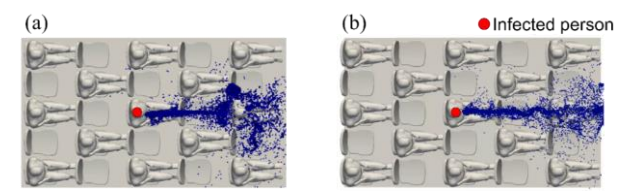


Fig. 10 Droplet dispersion in staggered conditions at (a) flat and (b) inclined seating arrangement, no-wind conditions.

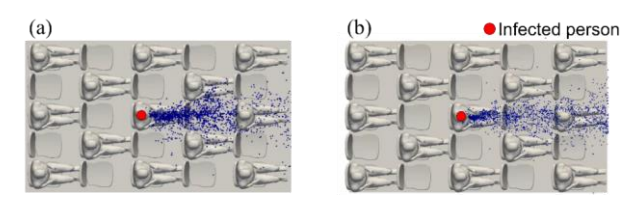


Fig. 11 Droplet dispersion in staggered conditions at (a) flat and (b) inclined environments, wind conditions from 0°.

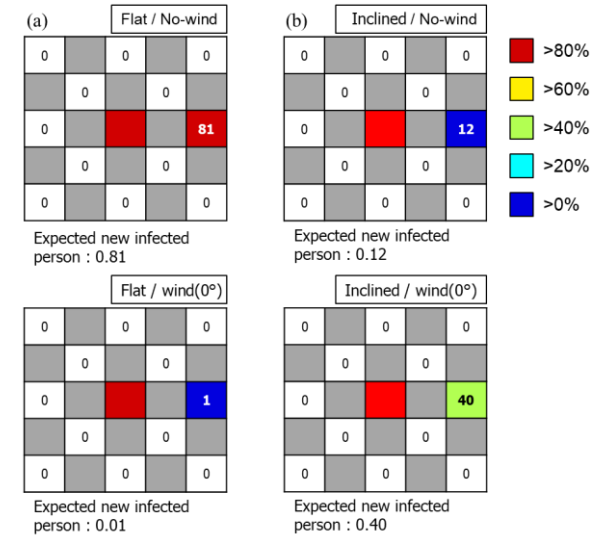


Fig. 12 Distributions of infection risk in staggered conditions at (a) flat and (b) inclined environment, no-wind (Top), and wind (Bottom) conditions.

9. Conclusion

In this study, we have investigated the droplet dispersion and infection risk in different seating arrangements and wind flow conditions as flat and inclined environments. To do that, we have presented a numerical framework developed for the simulation of large-scale droplet dispersion for COVID-19 type pandemic. The numerical results indicate that the dispersion of

droplets and infection risk are strongly dependent on the seating arrangement and wind direction by reducing the local concentration of droplets or spreading to other regions. Furthermore, the wind flow in different directions can also significantly affect the droplet dispersion and infection risk.

Thus, Proper seating arrangements can be effective in reducing the infection risk in two different environments and wind flow conditions. These findings can provide important insights for designing effectively to reduce infection risk in public places.

Acknowledgement: This work was supported by JST CREST, Grant Number JPMJCR20H7, Japan, and through the computing resources provided on the Fugaku supercomputer by the RIKEN Center for Computational Science and through the HPCI system research project (Project ID:hp220183)

Reference

- [1] Gralton, J., Tovey, E., McLaws, M.L., and Rawlinson, W.D. The role of particle size in aerosolised pathogen transmission: a review. *J. Infect.* 62(1), pp.1–13, 2011.
- [2] Gupta, J.K., Lin, C.H., and Chen, Q. Flow dynamics and characterization of a cough. *Indoor Air*. 19(6), pp.517–525, 2009.
- [3] Wei, J. and Li, Y. Airborne spread of infectious agents in the indoor environment. *Am. J. Infect. Control* 44(9), S102–S108, 2016.
- [4] Löhner, R., Antil, H., Idelsohn, S., and Oñate, E. Detailed simulation of viral propagation in the built environment. *Comput. Mech.* 66(5), pp.1093–1107, 2020.
- [5] Redrow, J., Mao, S., Celik, I., Posada J.A., and Feng, Z.G. Modeling the evaporation and dispersion of airborne sputum droplets expelled from a human cough. *Build. Environ.* 46(10), pp.2042–2051, 2011.
- [6] Bale, R., Wang, W.H., Li, C.G., Onishi, K., Uchida, K., Fujimoto, H., Kurose, R., and Tsubokura, M. A Scalable Framework for Numerical Simulation of Combustion in Internal Combustion Engines. *PACS'20*. pp.1–10, 2020.
- [7] Li, C.G., Tsubokura, M., and Bale, R. Framework for simulation of natural convection in practical applications. *Int. Commun. Heat Mass Transfer* 75, pp.52–58, 2016.
- [8] Kitano, T., Nishio, J., Kurose, R., and Komori, S. Effects of ambient pressure, gas temperature and combustion reaction on droplet evaporation. Combust. Flame, 161(2), pp.551–564, 2014.
- [9] Baba, Y. and Kurose, R. Analysis and flamelet modelling for spray combustion. *J. Fluid Mech.* 612, pp.45–79, 2008.
- [10] Nakamura, M., Akamatsu, F., Kurose, R., and Katsuki, M. 2005. Combustion mechanism of liquid fuel spray in a gaseous flame. Phys. Fluids, 17(12), 123301, 2005.

- [11] Miller, R.S., Harstad, K., and Bellan, J. Evaluation of equilibrium and non-equilibrium evaporation models for many-droplet gas-liquid flow simulations. Int. J. Multiph. Flow, 24(6), pp.1025–1055, 1998.
- [12] Bale, R., Li, C.G., Yamakawa, M., Iida, A., Kurose, R., Tsubokura, M., Simulation of droplet dispersion in COVID-19 type pandemics on fugaku. *PASC'21*, pp.1–11, 2021.
- [13] Nakahashi, K. Building-Cube Method for Flow Problems with Broadband Characteristic Length. Computational Fluid Dynamics 2002. Springer Berlin Heidelberg, pp.77–81, 2003.
- [14] Bale, R., Patankar, N.A., Jansson, N., Onishi, K., and Tsubokura, M. Stencil Penalty approach-based constraint immersed boundary method. Comput. Fluids, 200, 104457, 2020.
- [15] Bhalla, A.P.S., Bale, R., Griffith, B.E., and Patankar, N.A. A unified mathematical framework and an adaptive numerical method for fluid-structure interaction with rigid, deforming, and elastic bodies. J. Comput. Phys. 250, pp.446–476, 2013.
- [16] Liu, L., Wei, J., Li, Y., and Ooi, A. Evaporation and dispersion of respiratory droplets from coughing. *Indoor Air*. 27(1), pp.179–190, 2017.
- [17] Xie, X., Li, Y., Chwang, A.T.Y., Ho, P.L., and Seto, W.H. How far droplets can move in indoor environments-revisiting the Wells evaporation-falling curve. *Indoor air.* 17(3), pp.211–225, 2007.
- [18] Bale, R., Iida, A., Yamakawa, M., Li, C.G., and Tsubokura, M. Quantifying the COVID19 infection risk due to droplet/aerosol inhalation. Sci Rep 12, 11186, 2022.
- [19] Gupta, J.K. Lin, C.H., Chen, Q. Characterizing exhaled airflow from breathing and talking. *Indoor Air.* 20(1), pp.31–39, 2010.
- [20] Watanabe, T., Bartrand, T.A., Weir, M.H., Omura, T., and Haas, C.N. Development of a dose-response model for sars coronavirus. *Risk Anal. Int. J.* 30, pp.1129–1138, 2010.
- [21] Watanabe, T., Bartrand, T.A., Omura, T., and Haas, C.N. Dose-response assessment for influenza a virus based on data sets of infection with its live attenuated reassortants. *Risk Anal. Int. J.* 32, pp.555–565, 2012.
- [22] Prentiss, M., Chu, A., and Berggren, K.K. Superspreading events without superspreaders: Using high attack rate events to estimate N₀ for airborne transmission of COVID-19. MedRxiv, 2020.
- [23] Augenbraun, B.L., Lasner, Z.D., Mitra, D., Prabhu, S., Raval, S., Sawaoka, H., Doyle, J.M. Assessment and mitigation of aerosol airborne SARS-CoV-2 transmission in laboratory and office environments. *J. Occup. Environ. Hyg.* 17(10), pp.447–456, 2020.